

Supporting Information

A mechanically robust spiral fiber with ionic-electronic coupling for multimodal energy harvesting

Shengyang Zhou,^{1,2,} Yilin Zhang,¹ Xuan Li,¹ Chao Xu,² Joseph Halim,³ Shuai Cao,⁴*

Johanna Rosen,³ Maria Strömme²

¹ College of Materials Science and Engineering, Sichuan University, Chengdu 610065, Sichuan, China

² Nanotechnology and Functional Materials, Department of Materials Sciences and Engineering, The Ångström Laboratory, Uppsala University, Uppsala 751 03, Sweden

³ Materials Design, Department of Physics, Chemistry and Biology (IFM), Linköping University, Linköping 581 83, Sweden

⁴ Institute of High Performance Computing, Agency for Science, Technology and Research (A*STAR), 1 Fusionopolis Way, Connexis 138632, Singapore

* Email: shengyang.zhou@scu.edu.cn

Experimental Section

Materials. Poly (vinyl alcohol) (PVA) (M_w : 146000-186000, 99+% hydrolyzed), ionic liquid (IL) (1-Ethyl-3-methylimidazolium ethyl sulfate) were purchased from Sigma-Aldrich without any purification. MXene (Ti_3C_2) nanosheets (aqueous suspension) were prepared by previously reported methods as described below.

Preparation of MXene. The Ti_3AlC_2 MAX phase was synthesized using solid-liquid reaction of TiC (Alfa Aesar, 98+%), Ti (Alfa Aesar, 98+%) and Al (Alfa Aesar, 98+%) of molar ratio of 2:1.25:2.2, respectively as described previously.¹ The mixture was placed in an alumina crucible and inserted in a horizontal furnace. The furnace was heated to 1380 °C with a rate of 3 °C/min under 5 sccm Ar flow. The heating temperature was kept at 1350 °C for 2 h and then cooled down to room temperature at a rate of 3 °C/min. The lightly sintered product was crushed using a mortar and pestle and sieved through a 450-mesh sieve. To remove the excess Al, three grams of the powder was added to 40 ml of 12 M hydrochloric acid, HCl, (Fisher, Technical grade) and stirred using Teflon magnetic stirrer for 24 h (care was taken when adding the powder to HCl to avoid aggressive reaction, 0.5 g was added each time and left to react for 3 min before adding another 0.5 g). The mixture was washed with DI water for three cycles each of 40 ml, each time the mixture was centrifuged at 6000 rpm for 1 min followed by decanting of the supernatant. After washing the final mixture was filtered using vacuum filtration then the powder was left to dry in air overnight. One gram of the dried powder was added to a mixture of 12 ml HCl, 6 ml H_2O , and 2 ml HF and left under stirring for 24h at 35 °C.² Afterwards, the mixture was washed using deionized (DI) water, seven cycles of washing were performed each of 40 ml of water, and in each cycle MXene and water were added to a centrifuge tube, then hand shaken for 30 sec, then centrifuged at 6000 rpm for 1 min, then the supernatant was decanted. After the 7th cycle, the pH of the supernatant was checked to ensure that it is between 6 and 7. After washing, the final mixture was vacuum filtered to obtain the multilayered powder where 1 gram was then added to a LiCl solution (six grams of LiCl (Alfa Aesar, 98+%) dissolved in 25 ml of DI water) and stirred for 24h at room temperature. For delamination, the mixture was washed with DI water through several cycles each of 40 ml of water, the washing was stopped once a black supernatant was observed after centrifugation at 6000 rpm for 1 min. After that 40 ml of water were added to the sediment and was shaken for 5 min using the Vortex shaker at 1700 rpm followed by centrifugation for 1 h at 2500 rpm to obtain a supernatant of colloidal suspension of single to few layers of $Ti_3C_2T_x$.

Preparation of SMFs. The preparation of SMFs was initiated by fabricating of a bilayer thin film. The PVA powder was dissolved in deionized water (1 mg ml^{-1}) at $90 \text{ }^\circ\text{C}$ under string and circulation reflux. Then the IL was mixed thoroughly with PVA aqueous solution, which was thereafter drop-casted and volatilized into thin film using a polystyrene petri dish. In order to control the thin film to obtain uniform thickness, the petri dishes were floated on water that was placed in oven with $70 \text{ }^\circ\text{C}$ for overnight. Following that, the aqueous suspension of MXene (5 mg ml^{-1}) was dripped on the top of dried PVA/IL thin film in petri dish, which was then put in oven with $70 \text{ }^\circ\text{C}$ again for drying overnight. The obtained bilayer of MXene and PVA/IL was cut into square shape with different sizes, and scrolled into spiral fiber sheared by a polystyrene plastic board. The scrolled spiral fiber was further cold-drawn using a Shimadzu instrument (AGS-X) with a slow extension rate of 5 mm min^{-1} .

Characterization. The scanning electron microscopy (SEM) images were collected by using Zeiss Leo Gemini 1530 equipped with a field-emission gun at an accelerating voltage of 3 KV. The optical microscope photos were collected by using an Olympus optical microscope (AU03). The mechanical tensile stress-strain curves were recorded by using a Shimadzu instrument (AGS-X) at room temperature. The finite element analysis method was performed using ABAQUS 2021 software. The simulation of Nyquist plots was performed by using an open-access EIS-Lisa software. X-ray photoelectron spectroscopy (XPS) spectra were collected by using a PHI Quantera II instrument (Physical Electronics, USA), the pass energy was set as 50 eV with a step size of 0.1 eV for all the regions, the calibration of the XPS data was referred to the binding energy of C 1s peak. Fourier transform infrared (FTIR) spectra were recorded by using a spectrometer (PerkinElmer Lambda 900). X-ray diffraction patterns were collected by using a Bruker D8-power diffractometer. Pore size distribution and volume were calculated from nitrogen sorption isotherms that were measured by using a pore size and surface area analyzer (Micromeritics ASAP 2020) at 77 K. Before the measurements, all the samples were degassed at $100 \text{ }^\circ\text{C}$ under a kinetic vacuum ($<10^{-5} \text{ mmHg}$) for 12 h. Pore size distribution and volume were calculated by using the Micro-meritics ASAP 2020 software package. The electrical properties of SMFs were measured by an electrochemical workstation (CHI 660D) and a multi-meter (Hewlett Packard 34401A). Before the electrical test, the two side of the SMF were coated with silver paste to ensure a low contact resistance as shown in Figure S12 and Figure S16.

Supplementary Results and Discussion

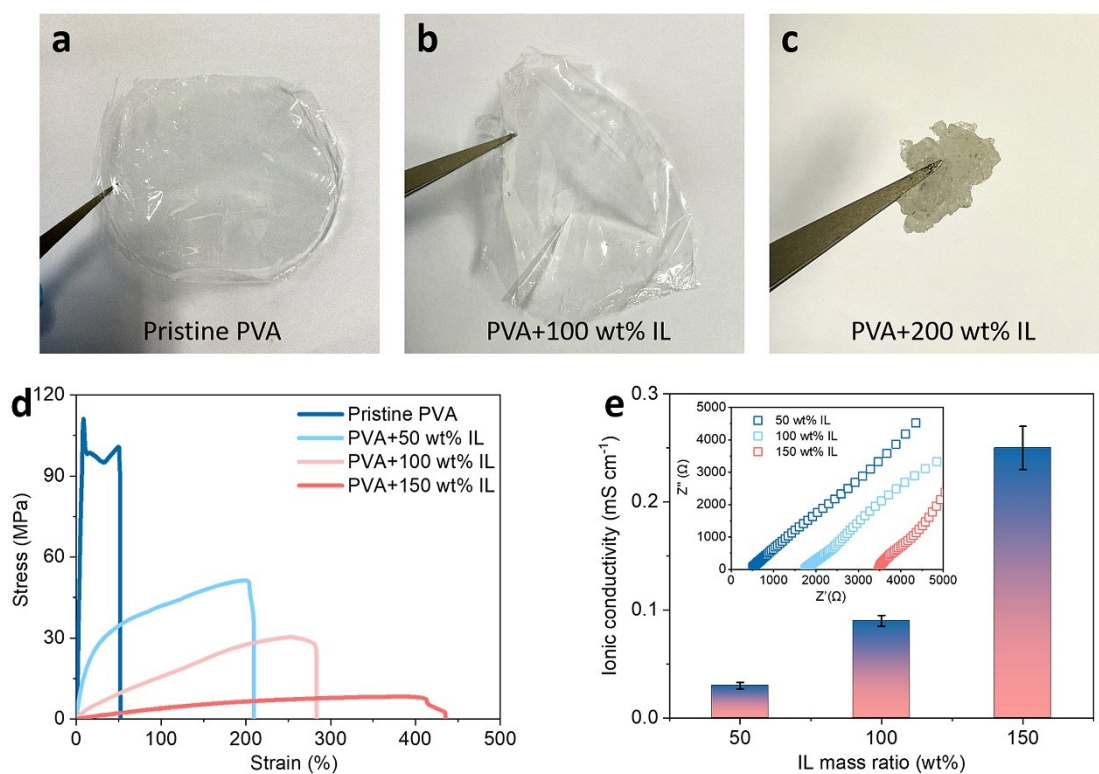


Figure S1. Characterization on solid polymer electrolyte used in this work. (a)-(c) Photos of PVA/IL film with different IL mass ratio. (d) Mechanical stress-strain curves of pristine PVA and PVA/IL with different IL mass ratio. (e) Ionic conductivity of PVA/IL with different IL mass ratio.

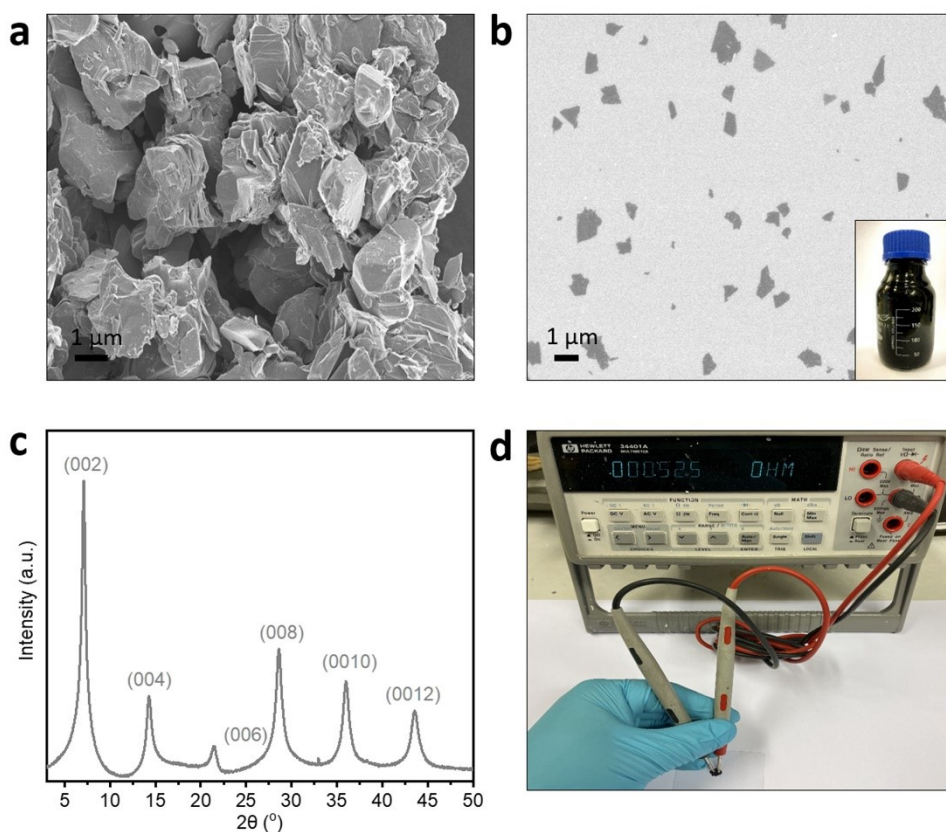


Figure S2. Characterization on MXene (Ti_2C_3) nanosheets studied in this work. SEM images of (a) MAX phase powder after etching by hydrofluoric acid, (b) monolayer MXene nanosheets after delaminating by lithium chloride. (c) XRD pattern of obtained monolayer MXene slurry. (d) Photo of resistance test on MXene thin film after drying to show their high electrical conductivity.

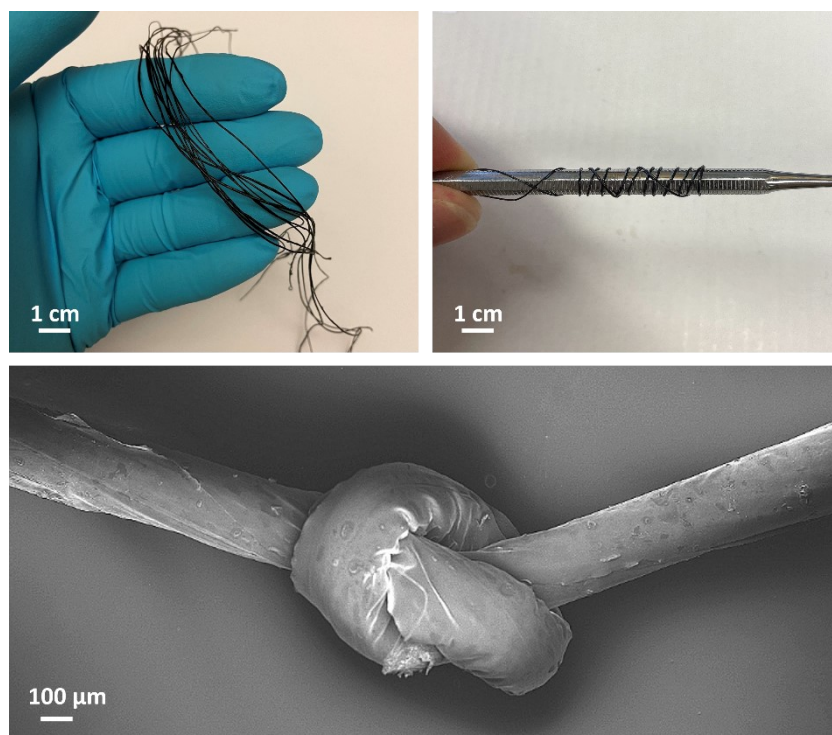


Figure S3. Photos and SEM image of cold-drawn SMFs showing their mechanical flexibility.

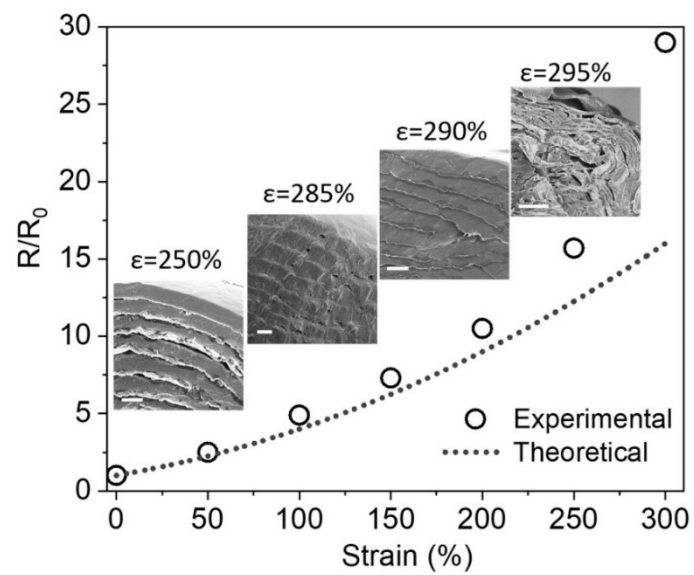


Figure S4. Comparison of the theoretical and experimental measured relevant electrical resistance (R/R_0) of SMFs at different strains during cold-draw process.

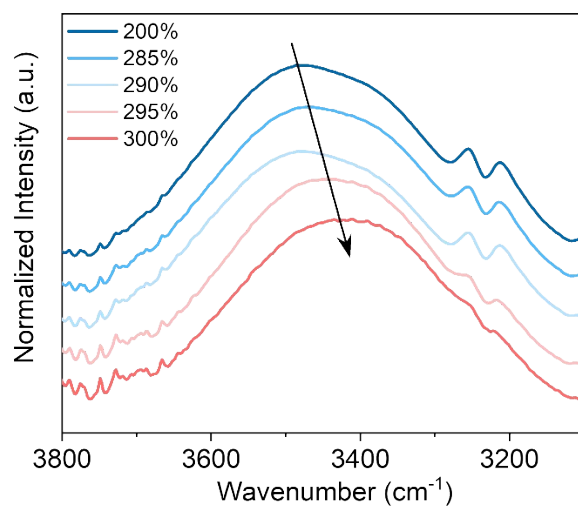


Figure S5. FTIR of SMFs during cold-draw under different elongation strains showing the breakage of hydrogen bonds during cold-draw when the strain is higher than 290%.

Table S1. Comparison on the toughness and specific Young's modules of SMF with other MXene-based materials that are reported recently.

Materials	Toughness (MJ m⁻¹)	Specific Young's modules (GPa m³ kg⁻¹)	References
Sequentially bridged MXene sheets	8.5	4.46	S3
PDDA and PVA composited MXene film	1.8	0.94	S4
NH ₄ ⁺ ions assisted wet-spinning MXene fiber	0.01	9.54	S5
Additive-Free MXene Liquid Crystal Fibers	0.35	2	S6
Aligned wet-spinning MXene fiber	1.07	5.2	S7
Highly aligned MXene film	10.9	8.5	S8
Nanocellulose composited MXene film	20.5	3.4	S9

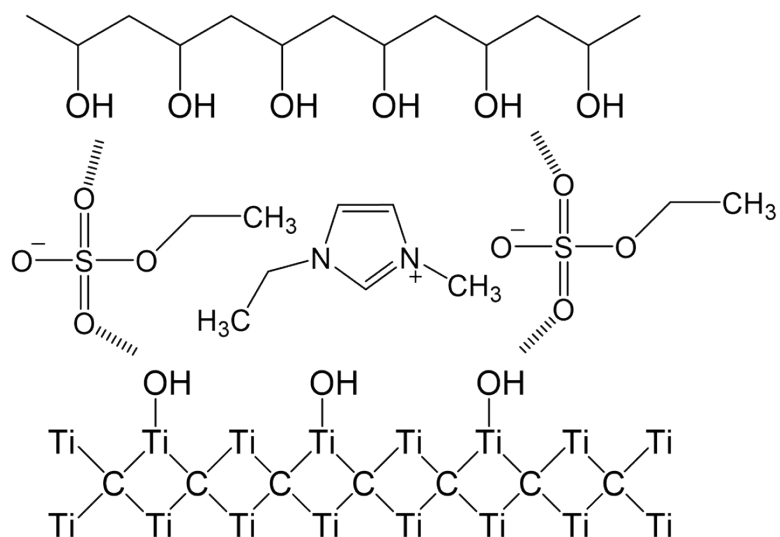


Figure S6. Schematic of the possible hydrogen bonds between MXene and PVA layer in SMFs.

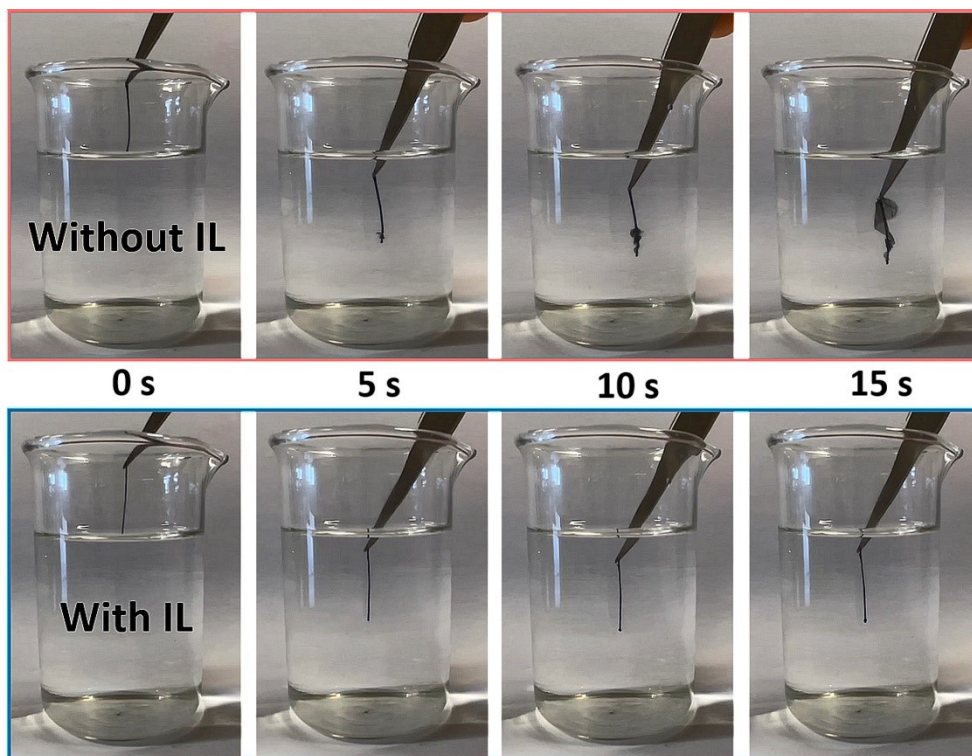


Figure S7. Photos of SMFs with and without IL in water showing the robustness and stability of SMFs with IL in water.

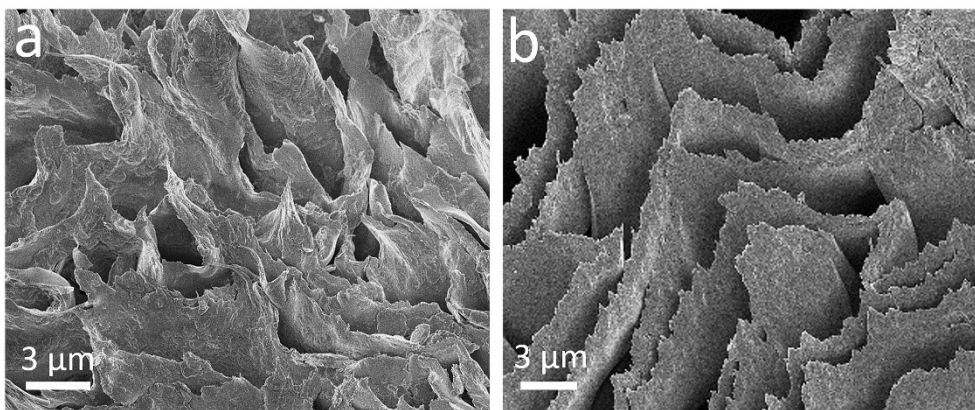


Figure S8. Cross-sectional SEM images of fracture of SMFs (a) with IL and (b) without IL showing the ductile fracture of cold-drawn SMFs with IL and brittle fracture of cold-drawn SMFs without IL.

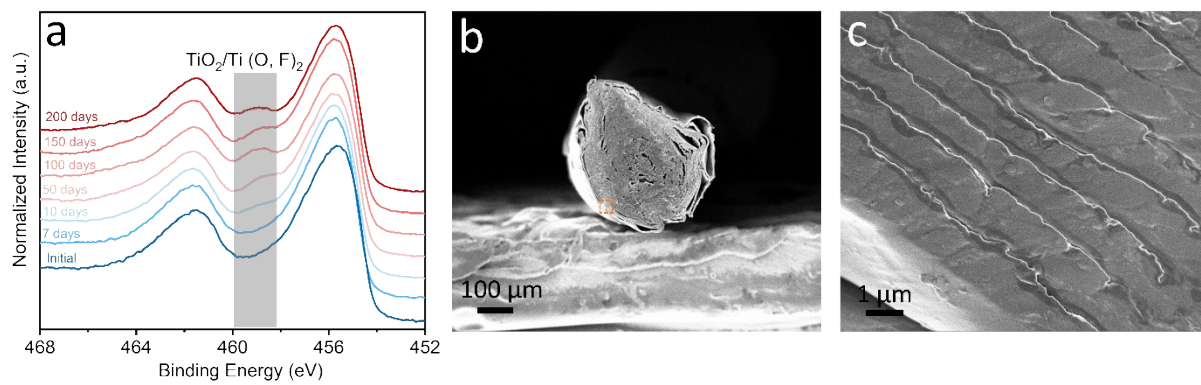


Figure S9. (a) X-ray photoelectron spectroscopy spectra (Ti 2p), (b-c) SEM images of SMFs collected in hundreds of days.

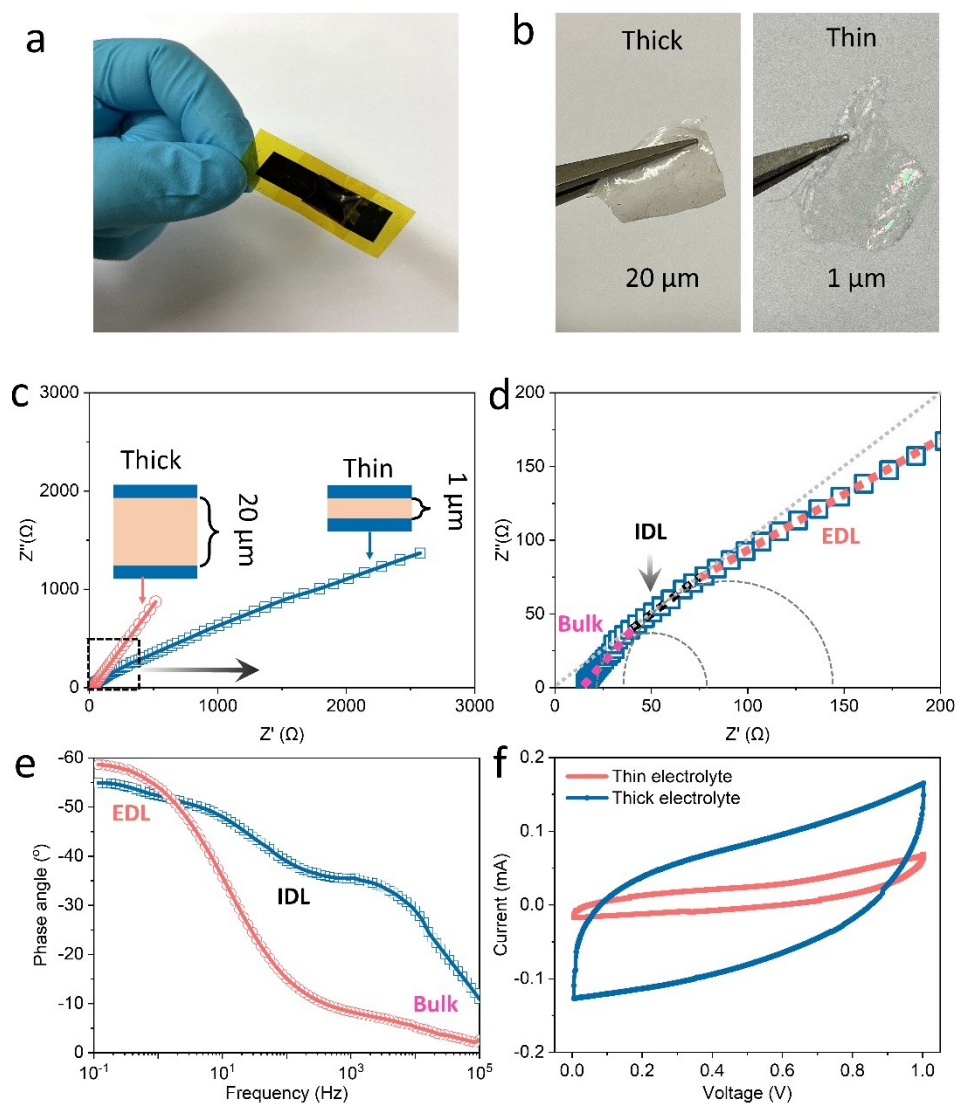


Figure S10. The designed comparative experiment by electrochemically characterizing the MXene-based symmetrical capacitor with different thickness of solid polymer electrolyte. (a) Photo of assembled symmetrical capacitor with typical MXene-polymer electrolyte-MXene sandwich structure. (b) Photos of PVA/IL solid polymer electrolyte with different thickness. (c) The Nyquist plots of symmetrical capacitor with different thickness of solid polymer electrolyte. (d) The identification of arc at medium frequency region belonging to the capacitance of IDL. (e) The Bode plots of symmetrical capacitor with different thickness of solid polymer electrolyte, the plateau of phase angle arises from the capacitance of IDL. (f) Cyclic voltammety of symmetrical capacitor with different thickness of solid polymer electrolyte, showing the decreased capacity of the device due to the formation of IDL in thin electrolyte.

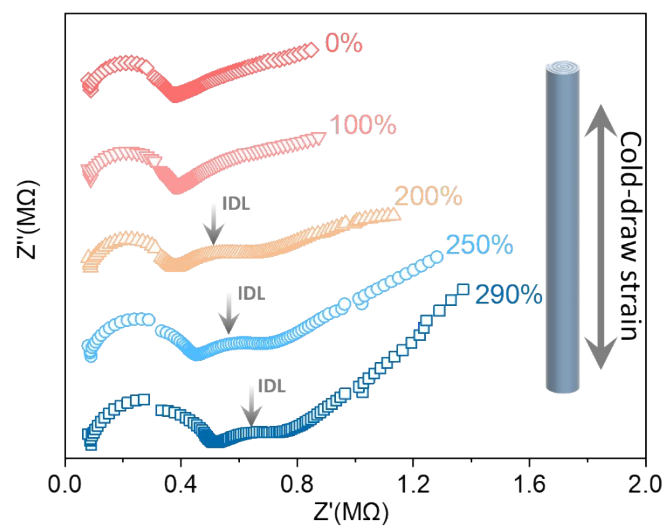


Figure S11. The Nyquist plots of SMFs at different strain during cold-draw process.

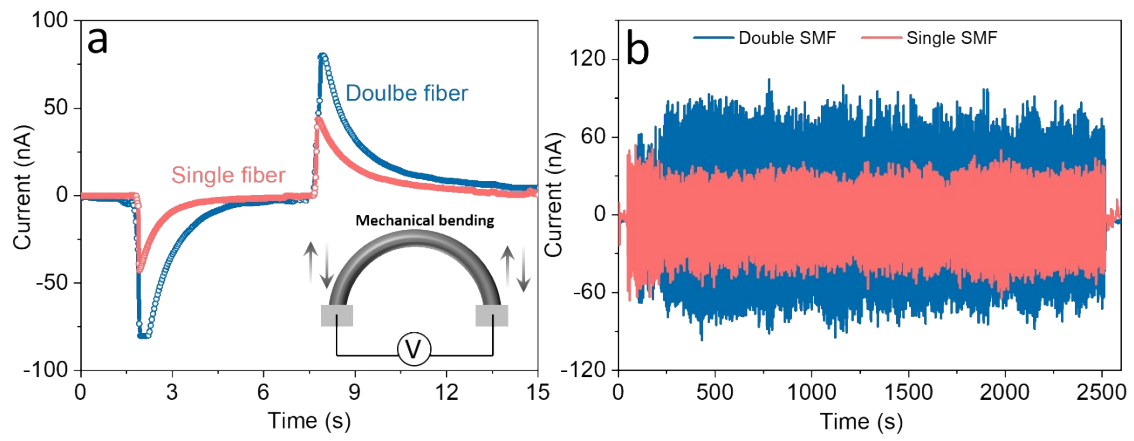


Figure S12. (a) The current output and delay of single and double SMFs under mechanical bending. (b) Current output of SMFs by a 500-cycle of bending test.

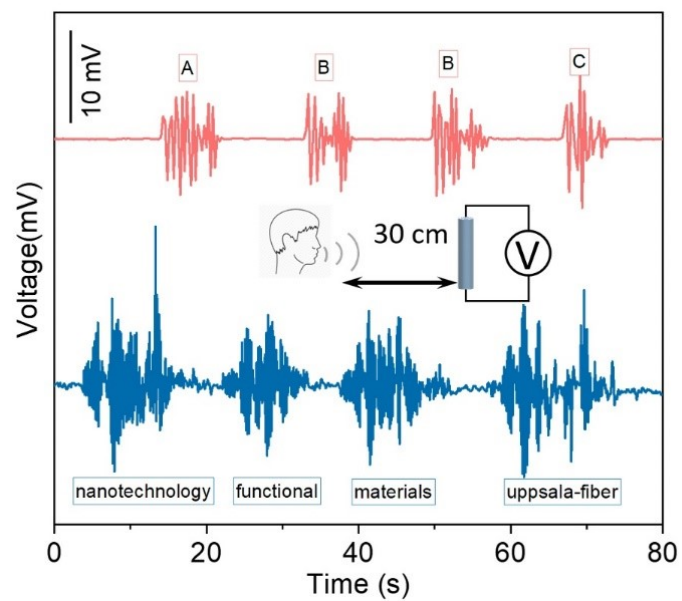


Figure S13. Voltage output of SMFs induced by human talking with different letters and words.

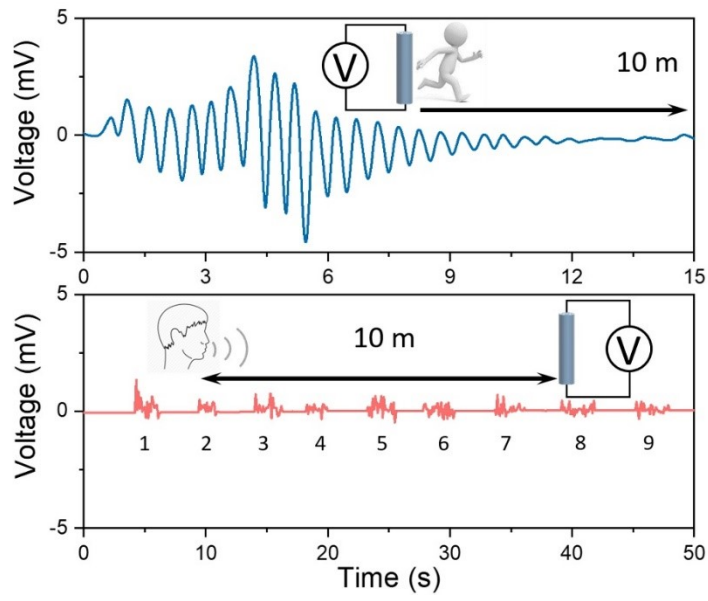


Figure S14. Voltage output of SMFs induced by human walking and talking in 10 meters away.

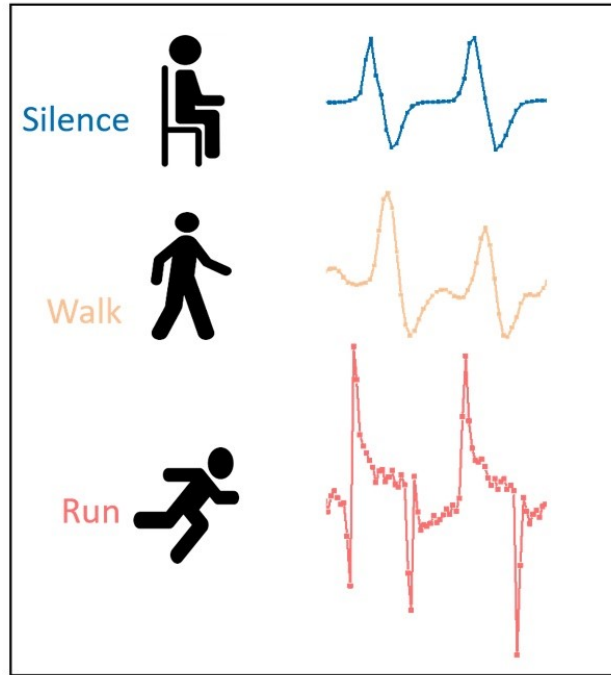


Figure S15. Electrocardiogram collected by SMFs under different states of human motion.

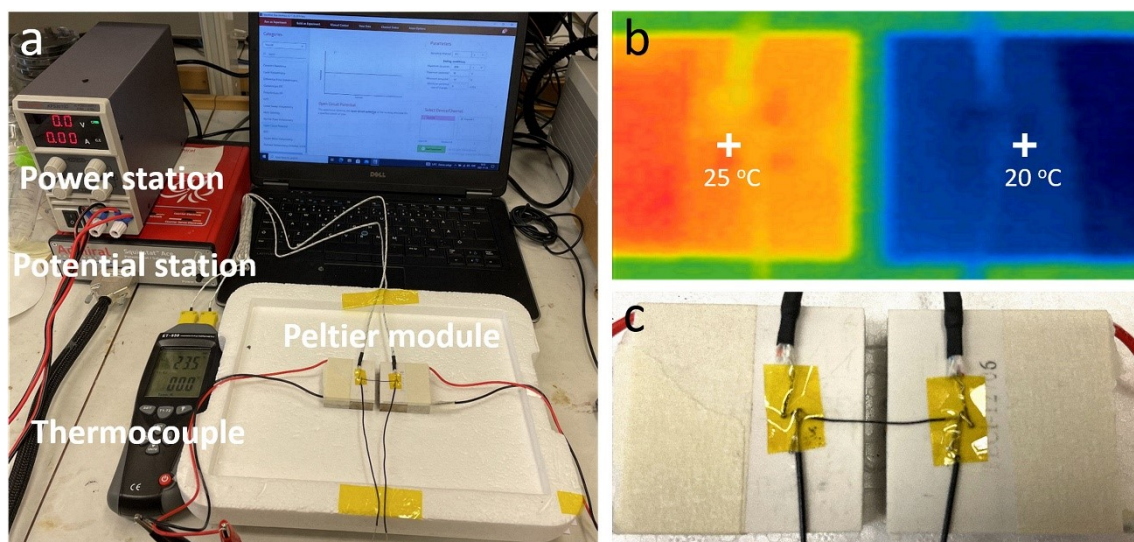


Figure S16. (a) Photo of the homemade apparatus for the measurement of thermoelectrical output of SMFs. (b) Infrared radiation image and (c) photo of two Peltier modules with a temperature difference of 5K.

Table S2. Comparison on the energy harvesting performance of SMFs with other materials reported recently.

Materials	Working mechanism	Performance	References
Ionic elastomers	Piezoionic effect	90mV 90nA	Adv. Mater. 2024, 2313127.
SMFs	Piezoionic effect	180mV 40nA	This work
Protein nanowires	Hydrovoltaic effect	0.5V 150nA	Nature 2020, 578, 550-554.
SMFs	Piezoionic-capacitive effect	40mV 5nA	This work
Gelatin gel	Ionic thermoelectric effect	17mV/K	Science 2020, 368, 1091-1098.
SMFs	Ionic thermoelectric effect	9mV/K	This work

Reference

1. Mathis, Tyler S., Kathleen Maleski, Adam Goad, Asia Sarycheva, Mark Anayee, Alexandre C. Foucher, Kanit Hantanasirisakul, Christopher E. Shuck, Eric A. Stach, and Yury Gogotsi. Modified MAX phase synthesis for environmentally stable and highly conductive Ti₃C₂ MXene. *ACS Nano* **2021**, *15*, 6420-6429.
2. Shuck, Christopher E., Asia Sarycheva, Mark Anayee, Ariana Levitt, Yuanzhe Zhu, Simge Uzun, Vitaliy Balitskiy, Veronika Zahorodna, Oleksiy Gogotsi, and Yury Gogotsi. Scalable synthesis of Ti₃C₂T_x mxene. *Advanced Engineering Materials* **2020**, *22*, 1901241.
3. Wan, Sijie, Xiang Li, Yanlei Wang, Ying Chen, Xi Xie, Rui Yang, Antoni P. Tomsia, Lei Jiang, and Qunfeng Cheng. Strong sequentially bridged MXene sheets. *Proceedings of the National Academy of Sciences* **2020**, *117*, 27154-27161.
4. Ling, Zheng, Chang E. Ren, Meng-Qiang Zhao, Jian Yang, James M. Giammarco, Jieshan Qiu, Michel W. Barsoum, and Yury Gogotsi. Flexible and conductive MXene films and nanocomposites with high capacitance. *Proceedings of the National Academy of Sciences* **2014**, *111*, 16676-16681.
5. Eom, Wonsik, Hwansoo Shin, Rohan B. Ambade, Sang Hoon Lee, Ki Hyun Lee, Dong Jun Kang, and Tae Hee Han. Large-scale wet-spinning of highly electroconductive MXene fibers. *Nature Communications* **2020**, *11*, 2825.
6. Zhang, Jizhen, Simge Uzun, Shayan Seyedin, Peter A. Lynch, Bilan Akuzum, Zhiyu Wang, Si Qin et al. Additive-free MXene liquid crystals and fibers. *ACS Central Science* **2020**, *6*, 254-265.
7. Shin, Hwansoo, Wonsik Eom, Ki Hyun Lee, Woojae Jeong, Dong Jun Kang, and Tae Hee Han. Highly electroconductive and mechanically strong Ti₃C₂T_x MXene fibers using a deformable MXene gel. *ACS Nano* **2021**, *15*, 3320-3329.
8. Zhang, Jizhen, Na Kong, Simge Uzun, Ariana Levitt, Shayan Seyedin, Peter A. Lynch, Si Qin et al. Scalable manufacturing of free-standing, strong Ti₃C₂T_x MXene films with outstanding conductivity. *Advanced Materials* **2020**, *32*, 2001093.
9. Cao, Jie, Zehang Zhou, Quancheng Song, Keyu Chen, Gehong Su, Tao Zhou, Zhuo Zheng, Canhui Lu, and Xinxing Zhang. Ultrarobust Ti₃C₂T_x MXene-based soft actuators via bamboo-inspired mesoscale assembly of hybrid nanostructures. *ACS Nano* **2020**, *14*, 7055-7065.